

Anomalous temperature dependence of optical and acoustic phonons in Bi_2Se_3 arising from stacking faults

Gyan Prakash,¹ Koushik Pal,² U. V. Waghmare,² and A. K. Sood¹

¹*Department of Physics and Center for Ultrafast Laser Applications,*

Indian Institute of Science, Bangalore 560012, India

²*Theoretical Sciences Unit, Jawaharlal Nehru Centre for*

Advanced Scientific Research, Jakkur campus, Bangalore 560064

Abstract

The class of layered 3D-topological insulators have shown intriguingly anomalous temperature dependence in their thermal expansion coefficients. It was proposed that stacking faults are the origin of the observed anomalous thermal expansion. Here, using femtosecond pump-probe differential reflectivity measurements we probe the carrier and coherently generated totally symmetric A_{1g} optical phonons in Bi_2Se_3 . Transient signals also show a low frequency ($\sim\text{GHz}$) oscillations due to coherent longitudinal acoustic phonons. We extract temperature dependence of optical constants, sound velocity and Young's modulus of Bi_2Se_3 using the strain pulse propagation model. A remarkable anomalous behavior around ~ 180 K is observed in the temperature dependence of optical and acoustic phonons as well as the optical constants. First-principles density functional theory (DFT) reveals that thermally activated formation of stacking faults is responsible for the anomalies observed in Bi_2Se_3 , similar to case of Sb_2Te_3 . We also show that inclusion of spin-orbit coupling plays an important role in reducing the total energy difference between the pristine and the faulted structures.

I. INTRODUCTION

Many compounds (e.g., Bi_2Se_3 , Bi_2Te_3 , hexagonal Sb_2Se_3 , $\beta\text{-As}_2\text{Te}_3$) in the group V-VI chalcogenide family have been shown to exhibit strong topological insulating phase [1–3] as well as excellent thermoelectric properties [4–8]. Hence, understanding the temperature dependence of structural, vibrational and electronic properties of these compounds are of paramount importance. Among the above compounds, Sb_2Te_3 [9, 10], Bi_2Se_3 [10] and Bi_2Te_3 [11] were shown to exhibit an intriguing temperature dependent anomaly in their linear thermal expansion coefficient along the trigonal c axis (α_{\parallel}). The coefficient α_{\parallel} exhibits a minimum at a certain temperature T_a ($T_a \sim 225$ K for Sb_2Te_3 , ~ 180 K for Bi_2Se_3 and ~ 240 K for Bi_2Te_3). Recently, our group [12] extensively studied the electron and phonon dynamics of Sb_2Te_3 by means of ultrafast pump-probe spectroscopy to shed light on the mechanisms responsible behind the observed structural and vibrational anomalies. In our earlier temperature dependent transient differential reflectivity study on Sb_2Te_3 we observed anomalous behavior in the relaxation dynamics of the photoexcited carriers, optical phonons and acoustic phonons corresponding to temperature associated with the anomalous thermal expansion [12]. Therein, we showed stacking fault as the origin of the anomaly and proposed that the same mechanism may be responsible for other materials in this class. The aim of the present work is to see if this is indeed the case or not. We take the case of Bi_2Se_3 from the same family of layered 3D TI and performed a combination of experimental and theoretical investigations. Using ultrafast pulses of photon energy ~ 1.57 eV, in a pump-probe experiment, we probe the carrier and phonon dynamics in Bi_2Se_3 in the temperature range 45 to 300 K with particular emphasis on exploring the effect of anomaly in the thermal expansion coefficient.

Pump induced electronic and thermal strain at the surface generates acoustic phonons [12–14]. Differential reflectivity signals of Bi_2Se_3 show clear oscillations related to acoustic phonons. Temperature dependent acoustic phonon frequency and decay time contain valuable information about structural transitions. Using strain pulse propagation model we extract the temperature dependence of the optical constants (n and k), sound velocity (v_{LA}) and Young’s modulus of elasticity (Y_{LA}). The obtained results show clear anomalous behavior of optical and acoustic phonons as well as the optical constants (n and k) around $T_a \sim 180$ K. Using first-principles density functional theory (DFT) calculations, we investi-

gate the origin of the observed anomalies through introducing stacking faults in the crystal structure of Bi_2Se_3 . Our results confirm the formation of the stacking fault as the generic mechanism responsible for the observed anomaly in various parameters in this class of materials. Spin-orbit coupling (SOC) is known to play an important role in strong topological insulators. Our results show that the SOC not only affects electronic topology, but also the energetics of different structures of these TIs. Inclusion of SOC reduces the total energy difference (at 0 K) between the pristine and the faulted structures. This total energy difference at 0 K (obtained with SOC) when combined with the difference of their vibrational contribution to the free energy, predicts a temperature of stabilization of stacking faults closer to the experimentally observed T_a .

II. EXPERIMENTAL DETAILS

Temperature dependent ultrafast differential reflectivity measurements were done in a continuous helium flow cryostat using pump and probe photons of energy 1.57 eV and pulse duration ~ 60 fs from a regenerative amplifier (Spitfire from Spectra-Physics) operating at 1 kHz repetition rate. Single crystal of Bi_2Se_3 was transferred into the evacuated cryostat immediately after cleaving the top surface to avoid any surface contamination. Pump-probe measurements were done with orthogonal polarized pump and probe beams with spot sizes of $850\ \mu\text{m}$ and $130\ \mu\text{m}$ at the overlap position, respectively. Analyzers orthogonal to pump beam were used to avoid pump scattering. The signal to noise ratio was improved by phase locked detection where the pump beam was modulated with a mechanical chopper and a lock-in-amplifier was slaved to this frequency. Pump and probe fluences were kept at $\sim 620\ \mu\text{J}/\text{cm}^2$ and $70\ \mu\text{J}/\text{cm}^2$ (much below the damage threshold of Bi_2Se_3), respectively for all the temperature dependent differential reflectivity measurement[15].

III. RESULTS AND DISCUSSION

A. Experimental Analysis

The layered crystal structure of Bi_2Se_3 is made up of close-packed atomic layers which are periodically stacked along the c-axis with a unit of five atomic planes ($\text{Se}^{(1)}\text{-Bi-Se}^{(2)}\text{-Bi-Se}^{(1')}$) called quintuple belonging to the space group symmetry $R\bar{3}m$ (No 166). Group theoretical

analysis of the symmetry of centrosymmetric rhombohedral (D_{3d}^5) crystal predicts 12 optical phonons at the Γ point with irreducible representations as $2A_{1g}(R)+2E_g(R)+2A_{2u}(IR)+2E_u(IR)$ [16], where R and IR refer to Raman and infrared active modes, respectively [16]. Fig. 1 (a) shows the differential reflectivity signal $\Delta R(t)/R_0$ obtained following pump excitation at 45 K. Transient kinetics clearly shows two superimposed oscillations of THz frequency corresponding to the coherent optical phonons. The frequencies of these superimposed oscillations are due to the displacive excitation [17, 18] of $A_{1g}^{(1)}$ and $A_{1g}^{(2)}$ optical phonon modes, confirmed by their oscillation frequencies of 2.23 THz and 5.29 THz observed at 45 K, respectively [16, 19]. As can be clearly seen from the transient $\Delta R(t)/R_0$ signal in Fig. 1(a), the low frequency mode $A_{1g}^{(1)}$ is long lived and is observed upto ~ 12 ps. The high frequency mode $A_{1g}^{(2)}$ is however, short lived and is observed upto ~ 5 ps only. A slow oscillation of GHz frequency together with an exponentially decaying background of carrier relaxation is also observed in the differential reflectivity signal of Bi_2Se_3 . The slow oscillation observed is due to the coherent acoustic phonon [13, 20].

As the higher frequency mode $A_{1g}^{(2)}$ is short lived, the amplitude, scattering rate, frequency and chirp of this mode are obscured by the underlying signal due to the electronic relaxation and the coherent acoustic phonon. To clearly observe and extract the temperature dependence of the physical parameters associated with the coherent optical phonons $A_{1g}^{(1)}$ and $A_{1g}^{(2)}$ in Bi_2Se_3 , we remove the signal originating from the electronic relaxation and the slow oscillation due to the coherent acoustic phonons by numerically differentiating the $\Delta R(t)/R_0$ data with respect to delay time at each temperature [18, 21–23]. The electronic and coherent acoustic phonon relaxations are analysed separately and discussed later. The obtained transient signal after taking the time derivative is proportional to the normal phonon coordinate $Q_0(t)$ of the coherent optical phonons [18, 22, 23]. A representative plot showing the time derivative of the $\Delta R/R_0$ signal at 45 K and its fast Fourier transform (FFT) are displayed in Fig. 1 (b) and (c), respectively. The FFT intensity of the $A_{1g}^{(1)}$ mode exhibits a symmetric Lorentzian lineshape. However, in contrast to the $A_{1g}^{(1)}$ mode the lineshape of the $A_{1g}^{(2)}$ mode is asymmetric. The asymmetric lineshape indicates the presence of chirp in the $A_{1g}^{(2)}$ mode [18, 22, 23].

We model the time derivative signal as sum of two chirped damping harmonic oscillators

[18, 23]

$$\frac{d(\Delta R/R_0)}{dt} = \sum_{i=1,2} B_i \exp(-\Gamma_i t) \cos [2\pi(\nu_i + \beta_i t)t + \phi_i] \quad (1)$$

TABLE I. The fitting parameters ν_{i0} , A_i , C_i and Γ_{i0} used in fitting the temperature dependence of scattering rates and frequencies of Bi₂Se₃ coherent optical phonons $A_{1g}^{(1)}$ and $A_{1g}^{(2)}$.

Optical phonon mode	ν_{i0} (THz)	A_i (THZ)	C_i (THZ)	Γ_{i0} (THz)
($i=1$) $A_{1g}^{(1)}$	2.237 ± 0.001	-0.0038 ± 0.0001	0.017 ± 0.001	0.149 ± 0.001
($i=2$) $A_{1g}^{(2)}$	5.49 ± 0.01	-0.001 ± 0.001	0.17 ± 0.01	0.32 ± 0.01

where B_i , Γ_i , ν_i and ϕ_i are the amplitude, scattering rate, frequency and initial phase of the coherent optical phonons $A_{1g}^{(1)}$ and $A_{1g}^{(2)}$, respectively. The parameter β_i is the chirp parameter describing the linear sweep in the phonon frequency with the pump-probe delay time. The indices $i=1$ and $i=2$ correspond to the optical phonon $A_{1g}^{(1)}$ and $A_{1g}^{(2)}$, respectively. Eq. (1) furnishes excellent fit to the time derivative data at all temperatures. The $A_{1g}^{(1)}$ optical phonon did not show chirp ($\beta_1 = 0$) at all temperatures. The chirp in the $A_{1g}^{(2)}$ optical phonon was found to be highest at 45 K ($\beta_2 = 2 \times 10^{-2}$ THz ps⁻¹), which decreased as the sample temperature was raised and completely disappeared for temperatures above 105 K (inset of Fig. 1 (c)). A fit to the time derivative data at 45 K is shown in panel (b) of Fig. 1. As shown in Fig. 1(c) the FFT of fitted curve in time-domain also captures the dynamics of the $A_{1g}^{(1)}$ and $A_{1g}^{(2)}$ modes in frequency-domain.

The optical phonon parameters obtained from the fit at all temperatures are shown in Fig. 2 (a-c) and Fig. 3 (a-c). We fit the amplitudes B_i (Fig. 2 (a) and 3 (a)) and scattering rates Γ_i (Fig. 2 (b) and 3 (b)) of $A_{1g}^{(1)}$ and $A_{1g}^{(2)}$ optical phonons with functions $B_i \sim \frac{n(\nu_{i0})+1}{2n(\nu_{i0}/2)+1}$ and $\Gamma_i(T) = \Gamma_{i0} + C_i [2n(\nu_{i0}) + 1]$ based on simple cubic anharmonic decay model [24], respectively. The parameter Γ_{i0} is the disorder-induced temperature-independent decay rate, C_i is related to phonon-phonon interaction and $n(\nu_{i0}) = \exp \left[\left(\frac{h\nu_{i0}}{k_B T} - 1 \right) \right]^{-1}$ is the Bose-Einstein statistical factor with indices $i=1$ and $i=2$ corresponding to $A_{1g}^{(1)}$ and $A_{1g}^{(2)}$ optical phonons with frequencies ν_{10} and ν_{20} , respectively. It can be seen that the amplitudes of the $A_{1g}^{(1)}$ and $A_{1g}^{(2)}$ optical phonons are anomalously high near the anomaly temperature $T_a \sim 180$ K ($A_{1g}^{(1)}$ amplitude is $\sim 58\%$ and $A_{1g}^{(2)}$ amplitude is $\sim 45\%$ higher than the value expected from the cubic anharmonic fit). The scattering rates of both $A_{1g}^{(1)}$ and $A_{1g}^{(2)}$ optical phonons

are also higher than the scattering rates predicted by the cubic anharmonicity model near the anomaly temperature $T_a \sim 180$ K. The increased scattering rate is also confirmed by the accompanied linewidth increase clearly seen in the FFT intensity of the $A_{1g}^{(1)}$ and $A_{1g}^{(2)}$ optical phonon, as shown in Fig. 2 (d) and 3(d). The enhanced phonon scattering rates (Γ_1 and Γ_2) near T_a is similar to the case of Sb_2Te_3 [12], arising from softness of the lattice in the temperature range near T_a .

The temperature dependent frequency shift in simple cubic anharmonic model is given by $\nu_i(T) = \nu_{i0} + A_i [2n(\nu_{i0}) + 1]$ where A_i is related to the phonon-phonon interaction. A more accurate description to temperature dependent frequency shift is given by including the quasi-harmonic contribution due to volume expansion [19, 25–27]: $\nu_i(T) = \nu_{i0} + A_i [2n(\nu_{i0}) + 1] + \nu_{i0} \left[\exp \left(-\gamma \int_0^T [\alpha_{\parallel}(T') + 2\alpha_{\perp}(T')] dT' \right) - 1 \right]$ where, γ is mode Grüneisen parameter, α_{\parallel} and α_{\perp} are the coefficients of thermal expansion along the ‘a’ and ‘c’ axis of the hexagonal lattice, respectively. We fit the frequency shift of $A_{1g}^{(1)}$ and $A_{1g}^{(2)}$ with temperature (Fig. 2 (c) and Fig. 3 (c)) by including the contribution due to cubic anharmonicity as well as quasi-harmonic. To capture the effect of anomalous thermal expansion on phonon frequencies, we used the experimental values of $\alpha_{\parallel}(T)$ and $\alpha_{\perp}(T)$ from Ref. [30] and mode Grüneisen parameter $\gamma=1.4$ [10] to calculate the quasi-harmonic contribution to frequency shift of both $A_{1g}^{(1)}$ and $A_{1g}^{(2)}$ optical phonons. The resulting fits are shown in Fig. 2(c) and 3(c). Table (I) summarizes the fit parameters. It can be seen that the temperature dependence of $A_{1g}^{(1)}$ and $A_{1g}^{(2)}$ mode frequencies, well captured by the anharmonic model, do not show a clear decrease in phonon frequency near T_a , probably due to larger error bars.

To extract the information about the temperature dependence of the photoexcited carriers and the coherent acoustic phonons in Bi_2Se_3 , we fit the $\Delta R(t)/R_0$ data with the following equation convoluted with a Gaussian laser pulse, at each temperature:

$$\begin{aligned} \frac{\Delta R(t)}{R_0} = & A_e \exp(-t/\tau_e) \\ & + \sum_{i=1,2} B_i \exp(-\Gamma_i t) \sin[2\pi(\nu_i + \beta_i t)t + \phi_i] \\ & + B_{LA} \exp(-t/\tau_{LA}) \cos(2\pi\nu_{LA}t + \phi_{LA}) + A_{off} \end{aligned} \quad (2)$$

where A_e and τ_e^{-1} are the amplitude and electron-phonon mediated relaxation rate of photoexcited carriers, respectively. A_{off} is the unrecovered background associated with the

diffusion of localized photoexcited carriers and their recombination [28]. B_i (B_{LA}), Γ_i (τ_{LA}), ν_i (ν_{LA}) and ϕ_i (ϕ_{LA}) are the amplitude, scattering rate (decay time), frequency and the phase of the coherent optical (acoustic) phonons, with the indices $i = 1, 2$ and LA corresponding to optical phonon $A_{1g}^{(1)}$, $A_{1g}^{(2)}$ and the longitudinal acoustic phonon, respectively. β_i is the chirp parameter of the optical phonons. While fitting the $\Delta R/R_0$ signal the optical phonon parameters Γ_i , ν_i , ϕ_i and β_i were fixed to the values obtained by fitting the time-derivative signal (Eq. 1). The amplitude B_i was scaled to get the best fit. Fig. 4 (a) shows the fit to the experimental data at 45 K with Eq. (2). The temperature dependence of the parameters related to the carrier relaxation A_e , τ_e^{-1} and A_{off} are shown in Fig. 4 (b-d). The electronic relaxation time (τ_e) is $\sim 1.5 \pm 0.3$ ps at 300 K, similar to the earlier reported results in Bi_2Se_3 thin films [28]. As shown in Fig. 4 (c) τ_e does not show any variation with temperature. However, the amplitudes $|A_e|$ and $|A_{off}|$ show a significant increase around ~ 180 K (Fig. 4 (b) and (d)), similar to the results in Sb_2Te_3 [12]. The changes in $|A_e|$ and $|A_{off}|$ are related to the temperature dependent reflectivity, discussed as follows.

Fig. 5 (b), (c) and (d) shows the amplitude, decay time and the frequency of the coherent acoustic phonon obtained by fitting $\Delta R/R_0$ with Eq. (2). Reflectivity of the Bi_2Se_3 sample at 1.57 eV, shown in Fig. 5 (a), was obtained by recording the probe intensity keeping the pump beam blocked. We calculated the optical constants n and k , sound velocity (v_{LA}) and Young's modulus of elasticity (Y_{LA}) from the experimental acoustic phonon parameters and the reflectivity using strain pulse propagation model [12–14]. The procedure adopted is as follows. The change in probe reflectivity owing to strain pulse is given by [12, 13]

$$\Delta R \propto \cos \left(\frac{4\pi n v_{LA} t}{\lambda} - \delta \right) e^{-z/\xi} \quad (3)$$

where δ is the phase shift, v_{LA} sound velocity, n refractive index, $\xi = \lambda/4\pi k$ is probe absorption length and λ is the probe wavelength. The longitudinal acoustic phonon frequency is given by $\nu_{LA} = 2n v_{LA}/\lambda$. The damping time is related to the duration the strain pulse takes to travel a distance equal to the penetration length of the probe pulse, $\tau_{LA} = \xi/v_{LA}$. From above relations we have $n/k = 2\pi \nu_{LA} \tau_{LA}$. For normal incident light, reflectivity is given by $R(T) = [(n-1)^2 + k^2] / [(n+1)^2 + k^2]$. Using $R(T)$, $\nu_{LA}(T)$ and $\tau_{LA}(T)$ we obtain refractive index $n(T)$ and $k(T)$. The longitudinal modulus of elasticity related to LA modes along the c-axis is given by $Y_{LA}(T) = v_{LA}^2(T) \rho(T)$, where $\rho(T)$ is density calculated using

temperature dependence of the lattice parameters of Bi_2Se_3 [10]. The temperature dependence of physical parameters n and k , v_{LA} and Y_{LA} obtained from strain pulse propagation analysis are shown in Fig. 5 (e-h). We see that near the anomaly temperature $T_a \sim 180$ K there is a drop in the optical constants (n and k) (Fig. 5 (e) and (f)) and a anomalous increase in the sound velocity (v_{LA}) and Young's modulus (Y_{LA}) (Fig. 5 (g) and (h)) similar to that observed in Sb_2Te_3 [12].

B. Theoretical Analysis

To understand the physical mechanism responsible behind the anomaly, DFT calculations were performed using the QUANTUM ESPRESSO (QE) [29] code. We used ultrasoft pseudopotentials (USPP) treating the exchange-correlation energy functional with a generalized gradient approximation (GGA) [30]. Since Bi has a strong spin-orbit coupling (SOC), we included SOC (through using fully relativistic USPP) in the calculation of electronic properties. On the other hand, as the SOC does not change the phonon frequencies significantly, vibrational properties were obtained without the inclusion of SOC (using scalar relativistic pseudopotentials). We truncated the expansion of the Kohn-Sham wave functions and the charge density in plane wave basis with energy cut-offs of 60 Ry and 240 Ry, respectively. To perform the Brillouin zone integrations, we used $12 \times 12 \times 2$ uniform grid of k-points. The discontinuity of the occupation numbers of the electronic states across the band gap were smeared with the Fermi-Dirac distribution function. Phonon frequencies were obtained using the linear response theory as implemented within the PH [31] package of QE.

In layered materials, stacking faults can occur with a relatively less energy penalty. We explored the formation of SFs as a possible mechanism of the anomaly as was done for Sb_2Te_3 . Following Ref. [12], we introduced stacking faults in the basal plane of the hexagonal crystal structure (conventional unit cells) of Bi_2Se_3 , and constructed the pristine ($\vec{a}_0, \vec{b}_0, \vec{c}_0$) and faulted ($\vec{a}_{\text{SF}} = \vec{a}_0, \vec{b}_{\text{SF}} = \vec{b}_0, \vec{c}_{\text{SF}} = \vec{c}_0 + \frac{1}{3}\vec{a}_0 + \frac{2}{3}\vec{b}_0$) configurations. In the above expression, \vec{a}_0, \vec{b}_0 , and \vec{c}_0 denote the lattice vectors for the hexagonal unit cell. We calculated the free energy $F = E_{\text{tot}} + F_{\text{vib}}$ of these structures as a function of temperature within a harmonic approximation, where E_{tot} is the total energy (calculated with SOC at 0 K) and F_{vib} is the vibrational contribution to the free energy given by $F_{\text{vib}} = \frac{k_B T}{N_q} \sum_{iq} \log[2\sinh(\frac{\hbar\omega_{iq}}{2k_B T})]$, N_q being the total number of q points in the Brillouin zone, ω_{iq} is the frequency of the i -th

phonon mode with wave vector q obtained using DFT linear response calculations.

After the optimization of the cell parameters (lattice vectors and the atomic positions) of the pristine and faulted structures of Bi_2Se_3 using scalar relativistic USPPs, we relaxed the atomic positions of each configuration using fully relativistic USPP to take into account the effect of SOC on the electronic states. The inclusion of SOC significantly reduces the total energy difference (at 0 K) between the pristine and faulted structures compared to the energy difference obtained without SOC. The energy difference without SOC was 72 meV/fu unit which reduced to 7 meV/fu after the inclusion of SOC. Hence, E_{tot} (calculated with SOC) was added to F_{vib} (obtained without SOC) to determine F for each configuration of Bi_2Se_3 . The calculated free energy difference ($\Delta F = F(\text{faulted}) - F(\text{pristine})$) decreases with temperature and becomes negative at 145 K (see Fig. 6) indicating a transition from the pristine to the faulted structure. This means that the structure of Bi_2Se_3 with infinitely extensive SFs will form and stabilize above $T_a^{\text{calc}} = 145$ K.

We associate the theoretically estimate of $T_a^{\text{calc}} = 145$ K with the experimentally observed anomaly temperature $T_a = 180$ K and attribute the origin of the observed anomalies in the optical constants (n and k), sound velocity (v_{LA}) and Young's modulus of elasticity (Y_{LA}) around 180 K to the formation of stacking faults near the anomaly temperature, consistent with the previous study [12]. Our theoretical calculations on Bi_2Se_3 and earlier on Sb_2Te_3 establish firmly that the anomalous temperature dependence of the physical properties and associated vibrational anomalies are due to the ease of formation of stacking faults above a certain temperature.

IV. CONCLUSION

We have shown that the acoustic and optical phonons as well as the electronic relaxation dynamics in Bi_2Se_3 obtained using ultrafast time resolved pump-probe spectroscopy, exhibits anomalous temperature dependence in the temperature range associated with an intriguing anomaly observed earlier in the thermal expansion. Using strain pulse propagation model, we extract the temperature dependence of the optical constants (n and k), sound velocity (v_{LA}) and the Young's modulus (Y_{LA}), which also show anomalous behavior around 180 K. These anomalies are similar to that observed in Sb_2Te_3 . The stacking fault mechanism explaining the anomaly in Sb_2Te_3 is also the origin in Bi_2Se_3 . Our DFT calculations show

that inclusion of SOC is essential and plays an important role in reducing the total energy difference between the pristine and faulted structures of Bi_2Se_3 . The present work establishes that the anomalies in the thermal expansion, vibrational mode parameters, optical constants and their origin in the ease of forming stacking faults above a certain temperature are quite generic in nature in these layered 3D topological insulators. The presence of stacking faults at high temperatures should be considered in understanding their physical properties.

ACKNOWLEDGMENTS

AKS thanks Dr. Jayaraman for providing single crystals. AKS thanks DST for financial support. GP thanks Council of Scientific and Industrial Research (CSIR) for SRF. AKS thanks DST for support through J.C. Bose National Fellowship. UVW acknowledges support from a J. C. Bose National Fellowship, a Sheikh Saqr Fellowship and IKST-Bangalore.

-
- [1] Y. Xia, D. Qian, D. Hsieh, L. Wray, A. Pal, H. Lin, A. Bansil, D. Grauer, Y. S. Hor, R. J. Cava, *et al.*, **Nat. Phys.** **5**, 398 (2009).
 - [2] A. Bera, K. Pal, D. V. S. Muthu, S. Sen, P. Guptasarma, U. V. Waghmare, and A. K. Sood, **Phys. Rev. Lett.** **110**, 107401 (2013).
 - [3] K. Pal and U. V. Waghmare, **Appl. Phys. Lett.** **105**, 062105 (2014).
 - [4] B. Poudel, Q. Hao, Y. Ma, Y. Lan, A. Minnich, B. Yu, X. Yan, D. Wang, A. Muto, D. Vashaee, *et al.*, **Science** **320**, 634 (2008).
 - [5] T. Caillat, M. Carle, P. Pierrat, H. Scherrer, and S. Scherrer, **J. Phys. Chem. Solids** **53**, 1121 (1992).
 - [6] D. Wright, **Nature** **181**, 834 (1958).
 - [7] N. Hinsche, B. Y. Yavorsky, M. Gradhand, M. Czerner, M. Winkler, J. König, H. Böttner, I. Mertig, and P. Zahn, **Phys. Rev. B** **86**, 085323 (2012).
 - [8] T. Thonhauser, T. J. Scheideman, J. O. Sofo, J. V. Badding, and G. D. Mahan, **Phys. Rev. B** **68**, 085201 (2003).
 - [9] P. Dutta, D. Bhoi, A. Midya, N. Khan, P. Mandal, S. S. Shanmukharao, and V. Ganesan, **Appl. Phys. Lett.** **100**, 251912 (2012).

- [10] X. Chen, H. D. Zhou, A. Kiswandhi, I. Miotkowski, Y. P. Chen, P. A. Sharma, A. L. L. Sharma, M. A. Hekmaty, D. Smirnov, and Z. Jiang, *App. Phys. Lett.* **99**, 261912 (2011).
- [11] P. Y. Li, Y. L. Chen, D. J. Zhou, P. Chen, Y. Zhang, S. Q. Deng, Y. J. Cui, and Y. Zhao, *Acta Phys. Sin.* **63**, 117301 (2014).
- [12] G. Prakash, K. Pal, M. Jain, U. V. Waghmare, and A. K. Sood, *Phys. Rev. B* **96**, 075109 (2017).
- [13] C. Thomsen, H. T. Grahn, H. J. Maris, and J. Tauc, *Phys. Rev. B* **34**, 4129 (1986).
- [14] S. Kumar, L. Harnagea, S. Wurmehl, B. Buchner, and A. Sood, *Europhys. Lett.* **100**, 57007 (2012).
- [15] D. Hsieh, J. McIver, D. Torchinsky, D. Gardner, Y. Lee, and N. Gedik, *Phys. Rev. Lett.* **106**, 057401 (2011).
- [16] W. Richter, H. Köhler, and C. R. Becker, *Phys. Status Solidi B* **84**, 619 (1977).
- [17] H. Zeiger, J. Vidal, T. Cheng, E. Ippen, G. Dresselhaus, and M. Dresselhaus, *Phys. Rev. B* **45**, 768 (1992).
- [18] N. Kamaraju, S. Kumar, and A. K. Sood, *Europhys. Lett.* **92**, 47007 (2010).
- [19] Y. Kim, X. Chen, Z. Wang, J. Shi, I. Miotkowski, Y. P. Chen, P. A. Sharma, A. L. L. Sharma, M. A. Hekmaty, Z. Jiang, *et al.*, *App. Phys. Lett.* **100**, 071907 (2012).
- [20] S. Wu, P. Geiser, J. Jun, J. Karpinski, and R. Sobolewski, *Phys. Rev. B* **76**, 085210 (2007).
- [21] N. Kamaraju, S. Kumar, S. Saha, S. Singh, R. Suryanarayanan, A. Revcolevschi, and A. K. Sood, *Phys. Rev. B* **83**, 134104 (2011).
- [22] Y. Wang, X. Xu, and R. Venkatasubramanian, *App. Phys. Lett.* **93**, 113114 (2008).
- [23] A. Q. Wu, X. Xu, and R. Venkatasubramanian, *App. Phys. Lett.* **92**, 011108 (2008).
- [24] P. Klemens, *Phys. Rev.* **148**, 845 (1966).
- [25] E. Zouboulis and M. Grimsditch, *Phys. Rev. B* **43**, 12490 (1991).
- [26] W. J. Borer, S. S. Mitra, and K. V. Namjoshi, *Solid State Comm.* **9**, 1377 (1971).
- [27] C. Postmus, J. R. Ferraro, and S. S. Mitra, *Phys. Rev.* **174**, 983 (1968).
- [28] Y. D. Glinka, S. Babakiray, T. A. Johnson, M. B. Holcomb, and D. Lederman, *App. Phys. Lett.* **105**, 171905 (2014).
- [29] P. Giannozzi, S. Baroni, N. Bonini, M. Calandra, R. Car, C. Cavazzoni, D. Ceresoli, G. L. Chiarotti, M. Cococcioni, I. Dabo, A. Dal Corso, S. de Gironcoli, S. Fabris, G. Fratesi, R. Gebauer, U. Gerstmann, C. Gougoussis, A. Kokalj, M. Lazzeri, L. Martin-Samos,

- N. Marzari, F. Mauri, R. Mazzarello, S. Paolini, A. Pasquarello, L. Paulatto, C. Sbraccia, S. Scandolo, G. Sclauszero, A. P. Seitsonen, A. Smogunov, P. Umari, and R. M. Wentzcovitch, *J. Phys. Condens. Mat.* **21**, 395502 (2009).
- [30] J. P. Perdew, K. Burke, and M. Ernzerhof, *Phys. Rev. Lett.* **77**, 3865 (1996).
- [31] S. Baroni, S. De Gironcoli, A. Dal Corso, and P. Giannozzi, *Rev. Mod. Phys.* **73**, 515 (2001).

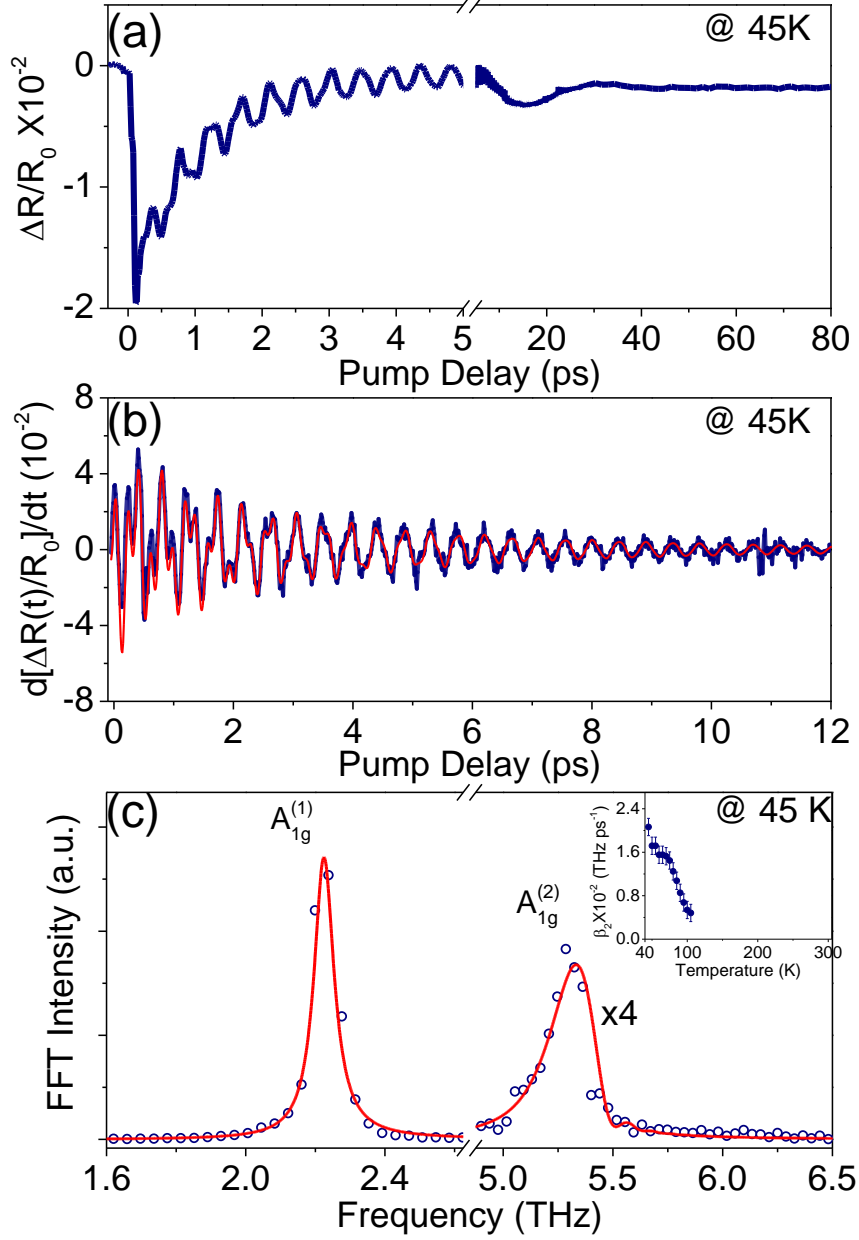


FIG. 1. Bi_2Se_3 pump-probe signal at 45 K (a) $\Delta R/R_0$ signal at 45 K showing transient oscillations due to two coherent optical phonons ($A_{1g}^{(1)}$ and $A_{1g}^{(2)}$) and an acoustic phonon over a background of electronic relaxation. (b) Time derivative of the pump-probe signal in (a). Solid line in red is fit to the experimental data. (c) FFT of the time derivative data and the fit in (b). Inset shows temperature dependence of the chirp parameter β_2 .

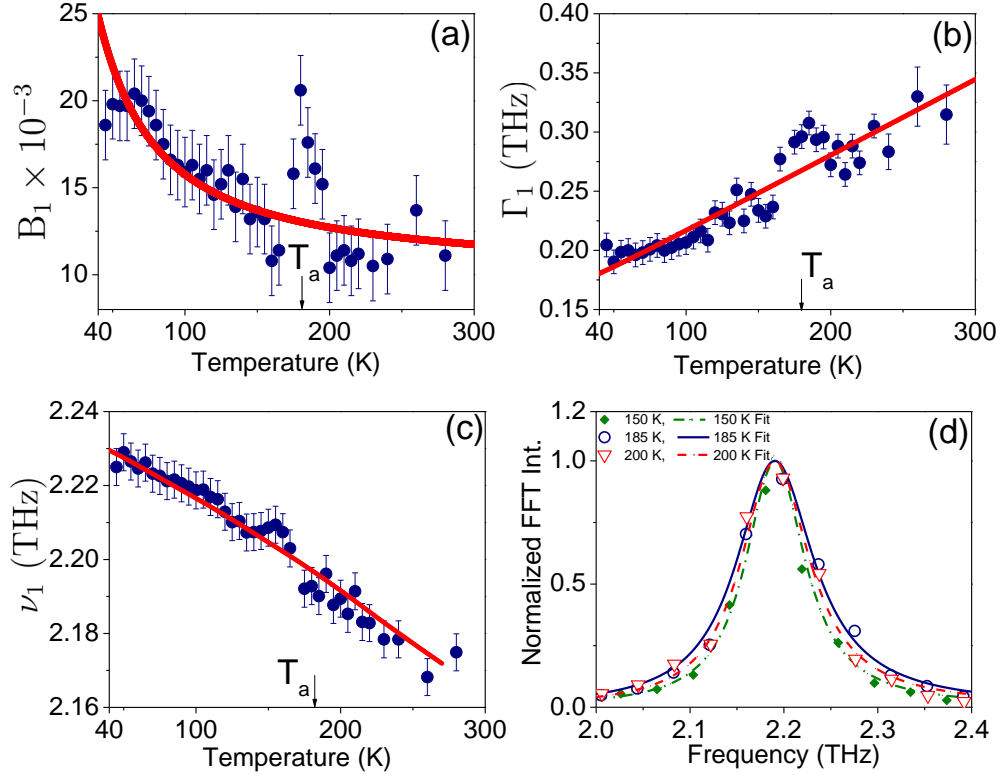


FIG. 2. Bi_2Se_3 coherent optical phonon $A_{1g}^{(1)}$. Temperature dependence of the (a) amplitude (b) scattering rate and (c) frequency shift of the Bi_2Se_3 coherent optical phonon $A_{1g}^{(1)}$. Solid line in (a) and (b) are fit to the data using cubic anharmonic model. Solid line in (c) is fit to the frequency shift including quasi-harmonic contribution along with the cubic anharmonic contribution. (d) FFT of the time derivative signal at temperatures 150 K, 185 K and 200 K for comparing the linewidth increase around the anomaly temperature $T_a \sim 180$ K. Frequencies of 150 K and 185 K plots are shifted to match FFT intensity maximum peak of the plot at 200 K for better comparison of the linewidth.

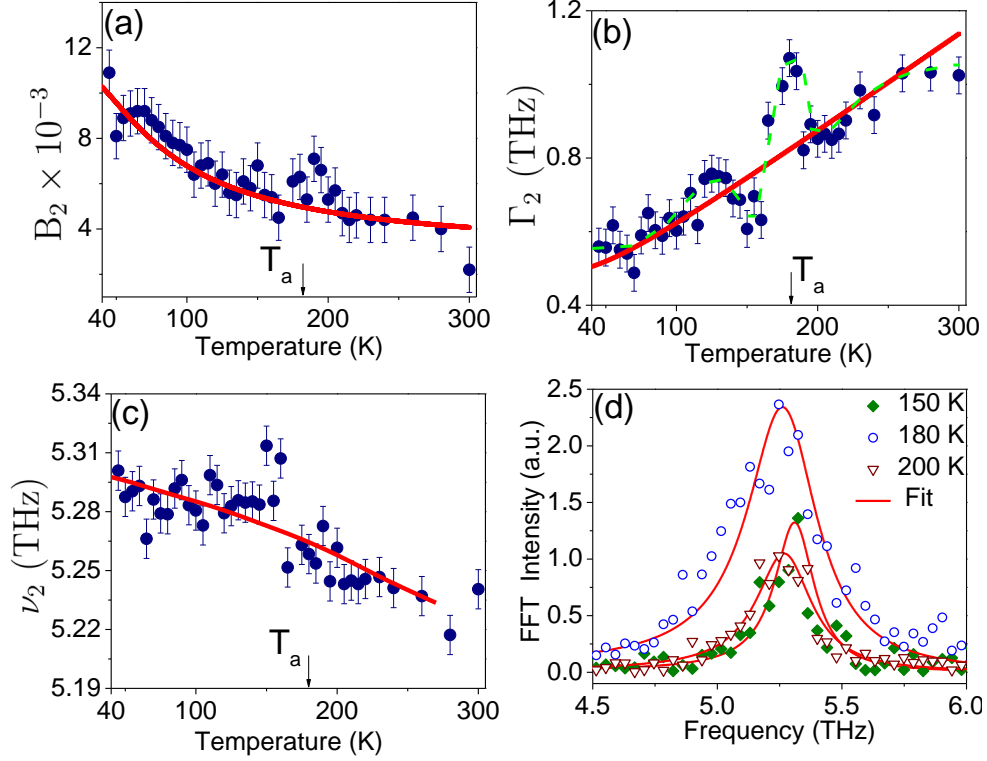


FIG. 3. **Bi_2Se_3 coherent optical phonon $A_{1g}^{(2)}$** . Temperature dependence of the (a) amplitude (b) scattering rate and (c) frequency shift of the Bi_2Se_3 coherent optical phonon $A_{1g}^{(2)}$. Solid line in (a) and (b) are fit to the data using cubic anharmonic model. Solid line in (c) is fit to the frequency shift including quasi-harmonic contribution along with the cubic anharmonic contribution. Dashed line in (b) through the data points in green color is guide to the eye. (d) FFT of the time derivative signal at three temperatures 150 K, 180 K and 200 K for comparing the linewidth increase around the anomaly temperature $T_a \sim 180$ K. Solid line in red is the FFT of the fit to the time derivative signal in time-domain.

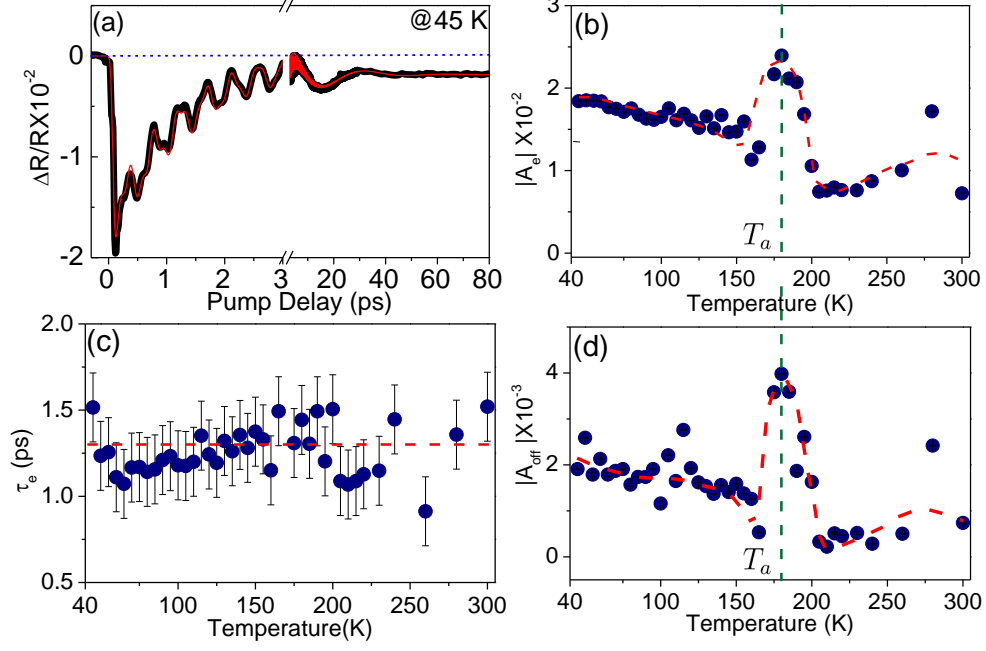


FIG. 4. **Electronic relaxation Bi_2Se_3** (a) $\Delta R/R_0$ signal at 45 K with fit to the experimental data as discussed in the text. Temperature dependence of electronic relaxation parameters obtained from the fit to the experimental $\Delta R/R_0$ signal: (b) amplitude, (c) relaxation time of electron-phonon mediated relaxation of photoexcited carriers and (d) amplitude of long time decaying background level. Dashed lines joining data points in (b), (c) and (d) are guide to eye. Error bars in (b) and (d) are smaller than the symbol size.

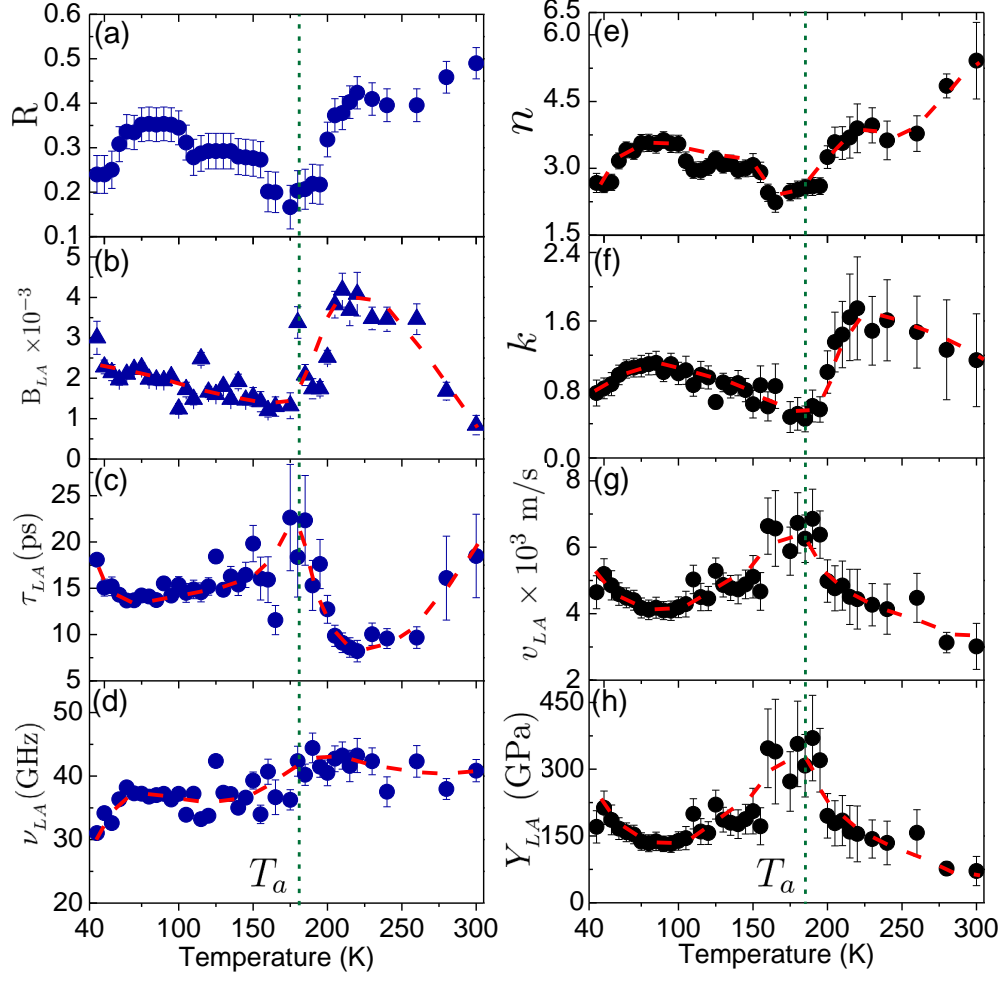


FIG. 5. **Bi₂Se₃ coherent longitudinal acoustic phonon.** (a) Temperature dependence of reflectivity of unexcited Bi₂Se₃ at 1.57 eV. (b) Acoustic phonon amplitude (B_{LA}), (c) dephasing time (τ_{LA}), (d) frequency (ν_{LA}), (e and f) optical constants (n and k), (g) sound velocity v_{LA} and (h) Young's modulus of elasticity (Y_{LA}). Dashed lines joining through the data points are guide to eye.

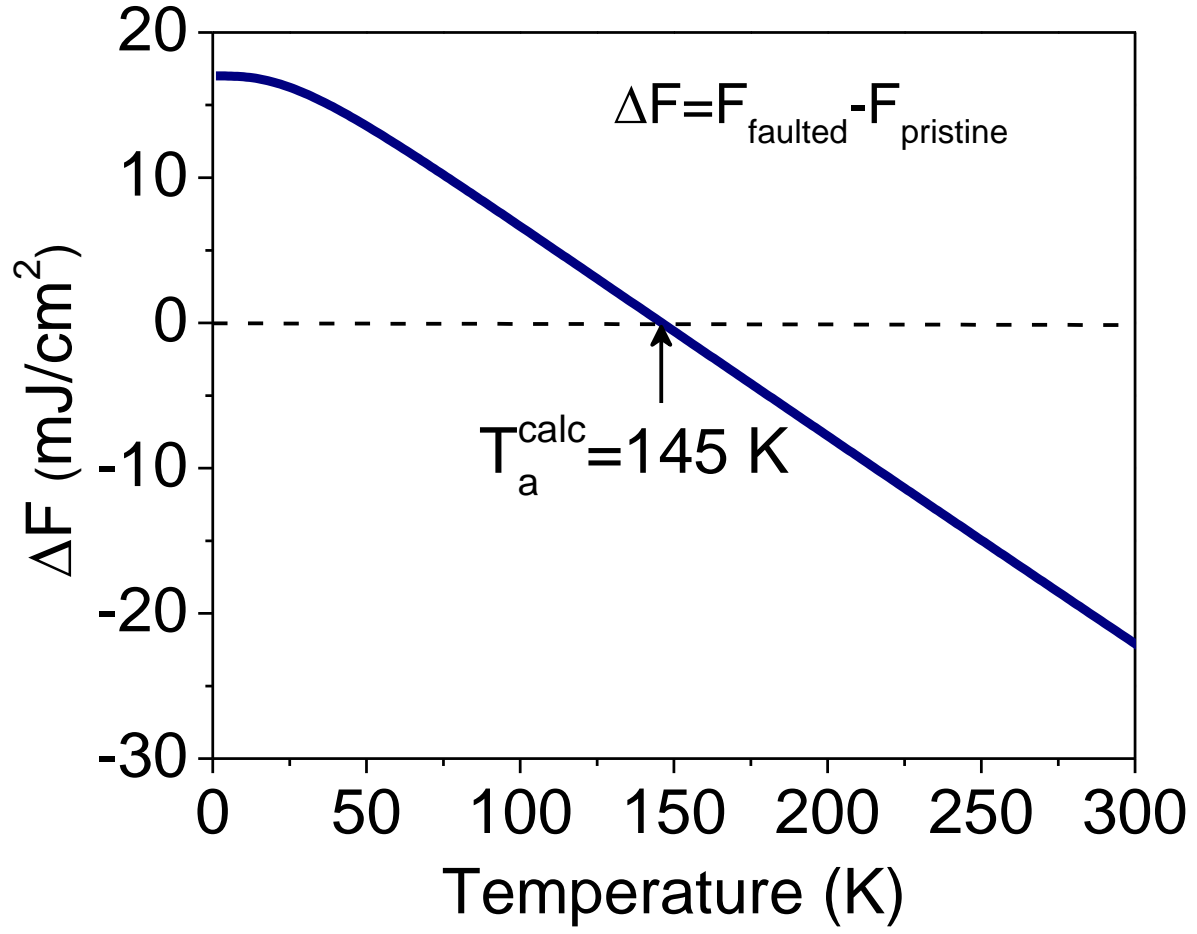


FIG. 6. Calculated free energy difference (ΔF) of the faulted and pristine structures of Bi_2Se_3 as a function of temperature.